Comparative study
of different functionalized graphene-nanoplatelet
aqueous nanofluids for solar energy applications

Javier P. Vallejo[1], Luca Mercatelli[2], Maria Raffaella Martina[2], Daniele Di Rosa[2,3],

Aldo Dell'Oro[4], Luis Lugo[1], Elisa Sani[2*]

[1]Departamento de Física Aplicada, Facultade de Ciencias, Universidade de Vigo, E-36310 Vigo,

Spain

[2]CNR-INO National Institute of Optics, Largo E. Fermi, 6, I-50125 Firenze, Italy

[3]University of Pisa, Department of Energy, Systems, Territory and Constructions Engineering

(D.E.S.T.eC.), Largo L. Lazzarino, I-56122 Pisa, Italy

[4]INAF, Osservatorio Astrofisico di Arcetri, Largo E. Fermi 5, I-50125 Firenze, Italy

*corresponding author: elisa.sani@ino.cnr.it

Abstract

The optical properties of nanofluids are peculiar and interesting for a variety of applications. Among them, the high light extinction coefficient of nanofluids can be useful in linear parabolic concentrating solar systems, while their properties under high light irradiation intensities can be exploited for direct solar steam generation. The optical characterization of colloids, including the study of non-linear optical properties, is thus a needed step to design the use of such novel materials for solar energy exploitation. In this work, we analysed two different types of nanofluids, consisting of polycarboxylate chemically modified graphene nanoplatelets (P-GnP) and sulfonic acid-functionalized graphene nanoplatelets (S-GnP) dispersed in water, at three concentrations from 0.005 wt% to 0.05 wt%. Moderately stable nanofluids were achieved with favourable light extinction properties, as well as a non-linear optical behaviour under high input solar intensities.

Keywords: direct absorption solar collectors; concentrating solar power; solar steam generation; nanofluids; graphene nanoplatelets; optical properties

1
2   **1. Introduction**
3
4
5   Nanofluids (i.e. suspensions of nanometer-sized solids in a base fluid) are receiving a huge
6   development in last years and are taken into account for a large variety of applications. Among the
7   fundamental characteristics of nanofluids, the knowledge of optical properties is needed for all
8   applications requiring the interaction of the nanomaterial itself with optical radiation. This field
9   results, in fact, really huge: from nanobiology/nanomedicine [1-4] to different types of optical sensors
10   [4-7], from the development of innovative light sources and optical components [3, 8] to nanomotors
11   [9, 10], just to mention few of them. Energy is one of the most appealing application fields of
12   nanofluids, and, in particular, dealing with optical properties, the solar energy exploitation. [11, 12].
13
14   As confirmed by the impressive growth of studies on this topic [13-16], dark nanofluids are
15   considered promising for the direct-absorption solar collector (DASC) scheme. DASCs offer several
16   advantages with respect to conventional surface-absorber architectures, because volumetric sunlight
17   absorption and heat exchange functions are carried out by the same element, namely the dark fluid,
18   arising in an optimized thermal transfer and in reduced thermal re-radiation losses. The DASC system
19   was originally proposed by Minardi and Chuang [17] in the mid-1970s to potentially enhance the
20   system efficiency by absorbing the energy within the fluid volume [18]. In particular, this was
21   typically done using India Ink, a black fluid composed by a suspension of micron-sized carbonaceous
22   particles prone to sedimentation and clogging of the pumps [13]. Moreover, black inks usually contain
23   organic and inorganic chromophores that show serious drawbacks because of their light-induced and
24   thermal degradation at the high operating temperatures. [18, 19]. Nanoparticles overcome these
25   critical issues and potentially increase the efficiency of DASCs. A large variety of nanoparticles and
26   base fluids has been investigated in the literature. Among them, the family of carbon-based
27   nanostructures has emerged as particularly promising. From carbon black [20] to graphite [21], as
28   well as single, multi-wall and functionalized nanotubes [22-24], carbon nanohorns [20, 25-27], many
29   nanofluids containing carbon nanoparticles have been studied for solar energy applications. Graphene
30   is one of most intriguing carbon allotropes [28, 29]. Graphene nanoplatelets or nanosheets consist of
31   small flakes of several-layer staked graphene that partially inherit the good properties of graphene
32   with much lower production costs. Graphene nanoparticles are naturally hydrophobic. They can be

1 stably suspended in water after chemical modifications of their surface, e.g. by oxidation or by

2 different types of functionalization [30, 31]

3   A second promising field of application of nanofluids in renewable energies is direct solar steam

4 generation. Steam production is of crucial importance for many applications including electricity

5 generation, energy storage, biomass processing, water desalination and sterilization [32-35]. Green

6 and renewable steam production by solar energy is thus an important topic of research [36], as an

7 example to bring technologies essential for life in off-grid areas and resource-poor locations. Typical

8 solar steam production systems are currently based on solar trough or solar tower architectures with

9 a surface or cavity solar absorber [37-39]. They work heating a bulk fluid to its boiling temperature

10 under high optical concentration. The steam generation efficiency is strongly connected to the surface

11 temperature and thermal radiation properties of the absorber. However, as bulk steam production

12 needs high temperatures, these conventional systems also suffer from high heat losses and low

13 efficiency. To overcome this drawback, a possibility is looking for solutions able to produce steam

14 without requiring heating the whole liquid volume to the boiling point. Different authors reported on

15 the efficient solar steam generation by different nanoparticles, such as gold [40-42], silicon [43] and

16 carbon nanostructures [44, 45].

17   For the solar steam production, the nanofluid must be subjected to intense light irradiation, as it

18 happens under high solar concentration regimes. It is important to notice that when materials are

19 maintained in such conditions, their response could be nonlinearly dependent on the input light

20 intensity. In this regime, basic optical properties like transmittance undergo a change, and the values

21 obtained under low input intensities are no more applicable. For this reason, a dedicated study must

22 to be carried out, to assess intensity-dependent optical properties as well.

23   The obtaining of homogeneous dispersions of the nanoadditives in the base fluids is still

24 nowadays a methodological challenge and this issue usually must be confronted [46]. The strong van

25 der Waals interactions between nanoparticles favour the creation of aggregates that tend to easily

26 settle because of their higher weights, leading to variations in the dispersion physical properties [47].

27 Different physical or chemical methods are usually employed to obtain stable samples as

28 ultrasonication, addition of surfactants, pH-modification or the surface modification of the particles

29 [46].

30   In this work, we report on the comparative characterization of linear and nonlinear optical

31 properties of graphene nanoplatelets showing two different functionalization types and suspended in

1 water. These suspensions were characterized through a stability analysis based on zeta potential and

2 dynamic light scattering (DLS) measurements. Then, we focused on the DASC application, assessing

3 the spectral extinction coefficient of aqueous nanofluids as a function of the nanoparticle

4 concentration. Finally, we investigated the nanofluid response to high intensity laser radiation, to

5 evaluate the potential of these nanoadditives for direct vapor generation and other nonlinear optics

6 applications.

7

8 **2. Experimental**

9

10 *2.1.Materials and sample preparation*

11

12 Polycarboxylate chemically modified graphene nanoplatelets, P-GnP, and Sulfonic acid-

13 functionalized graphene nanoplatelets, S-GnP, were supplied by NanoInnova Technologies S.L.

14 Madrid, Spain). Milli Q-grade water, W, was produced by a Milli-Q 185 Plus system (Millipore Ltd.,

15 Watford, UK) with a resistivity of 18.2 MΩ·cm.

16 For each nanopowder type, we prepared three aqueous suspensions, with nanoadditive concentrations

17 of 0.005 wt%, 0.025 wt% and 0.05 wt%. The proper amounts of nanopowder and base fluid were

18 weighted in a Mettler AE-200 balance (Mettler Toledo, Greifensee, Switzerland), with a 0.1 mg

19 uncertainty. After mixing and stirring, samples where submitted to ultra-sonication of 20 kHz

20 frequency during 120 min by means of an Ultrasounds ultrasonic bath (JP Selecta S.A., Barcelona,

21 Spain).

22

23 *2.2. Nanopowder characterization and stability*

24

25 The size and morphology of the nanoadditives were characterized by transmission electron

26 microscopy (TEM) over the employed nanopowders. TEM analyses were performed through a JEM-

27 2010F field emission electron microscope (JEOL, Tokyo, Japan), working at an operating accelerator

28 voltage of 200 kV. TEM images were obtained over drops of dispersions of each nanopowder in

29 analytical grade ethanol, placed over copper supports and previously dried at room temperature.

30 The stability of a dispersions can be analysed by UV–VIS spectroscopy, zeta potential analysis,

31 light scattering or electron microscopy, among other methods [46, 47]. In this work, zeta potential

1   and dynamic light scattering analyses were carried out to characterize the stability of the studied

2   samples by means of a Zetasizer Nano ZS (Malvern Instruments Ltd, Malvern, United Kingdom).

3   The zeta potential as a function of temperature was determined for the 0.025 wt% nanofluids in the

4   temperature range from 283.15 to 333.15 K. The evolution of the apparent size of the nanoadditives

5   as a function of the time after preparation for the 0.025 wt% nanofluids was also studied at 298.15 K

6   and using a scattering angle of 173°. Samples in static conditions from the preparation (hereinafter

7   "static" samples) and samples mechanically stirred previously to each measurement (hereinafter

8   "shaken" samples) were analysed. The stirring process applied to shaken samples previous to each

9   apparent size measurement was carried out at 2000 rpm during 1 min by means of a ZX3 Advanced

10 Vortex Mixer (VELP Scientifica SRL, Usmate Velate, Italy). Each value of zeta potential and

11 apparent size presented in this work was obtained as the average between three experimental tests.

12

13 *2.3. Optical characterization*

14

15   The optical properties of nanofluids were investigated both in linear conditions, obtaining the

16 spectral extinction coefficient, and under high intensity laser irradiation, assessing optical limiting

17 properties. Spectral optical transmittance in the linearity regime was measured using a double-beam

18 UV-VIS spectrophotometer (PerkinElmer Lambda900) using a variable length cell (50 - 500 μm) and

19 the method described elsewhere [48, 49]. High intensity experiments have been carried out using a

20 pulsed nanosecond Nd:YAG laser as light source (Quantel Q-smart 850, delivering 6 ns pulses at

21 1064, 532 and 355 nm wavelength, with 10 Hz repetition rate). The three laser emission wavelengths

22 were spatially separated by proper optical elements and focused on the sample by a lens of 300 mm

23 focal length. The sample was held in a quartz cuvette with 10 mm path length, put in a defocused

24 position to avoid cuvette damage. The beam exiting the sample was collected by a couple of lenses

25 of focal lengths 40 and 100 mm and focused on a pyroelectric detector (Ophir PE25C, Ophir PE9C).

26 The energy incident on the cuvette was varied and measured using a pyroelectric detector (Ophir

27 PE50BE, Ophir PE25C, Ophir PE9C). The laser experimental setup is sketched in Figure 1a and the

28 real image is shown in Figure 1b. It is worth to notice that our setup is different, and much simpler

29 than the conventional Z-scan technique. However its use in combination with semi-empirical models

30 allows to identify, in most cases, the active nonlinear process by a simple fitting procedure (see

31 below).

1

2

3

(a)

4
5
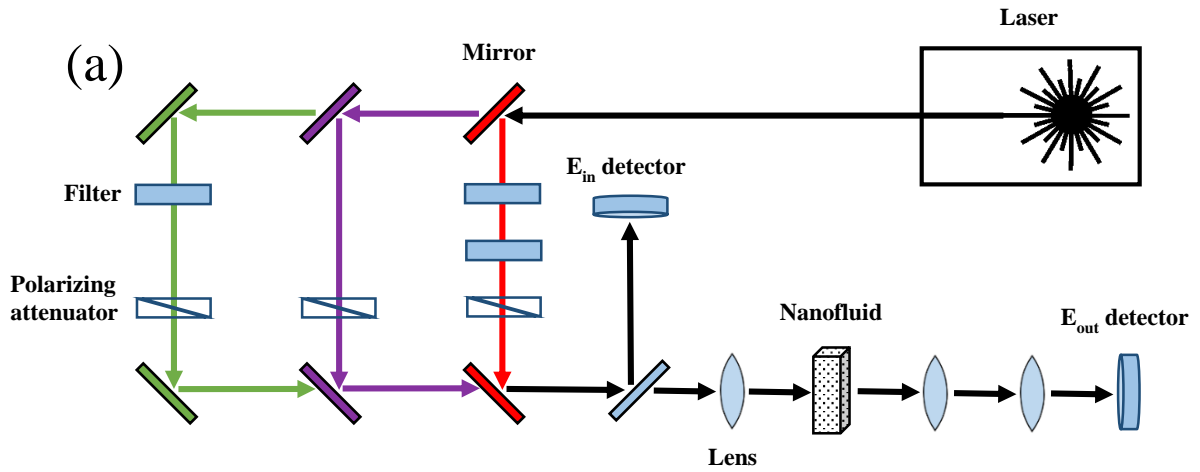
6
7
8   ***Figure 1***: *Scheme (a) and real image (b) of the laser experiment setup.*
9
10

11   **3. Results and discussion**

12

1   **3.1 Nanopowder characterization and stability**

2

3   TEM analysis results permit to settle the nanoplatelet structure of both nanoadditives, that is set

4   of stacked graphene layers, as it can be seen in Figure 2. S-GnP particles are generally larger than P-

5   GnP particles. As an example, Fig. 2a shows a S-GnP of around ~ 380 nm × ~ 590 nm and Fig. 2b

6   shows a P-GnP of around ~ 100 nm × ~ 210 nm.
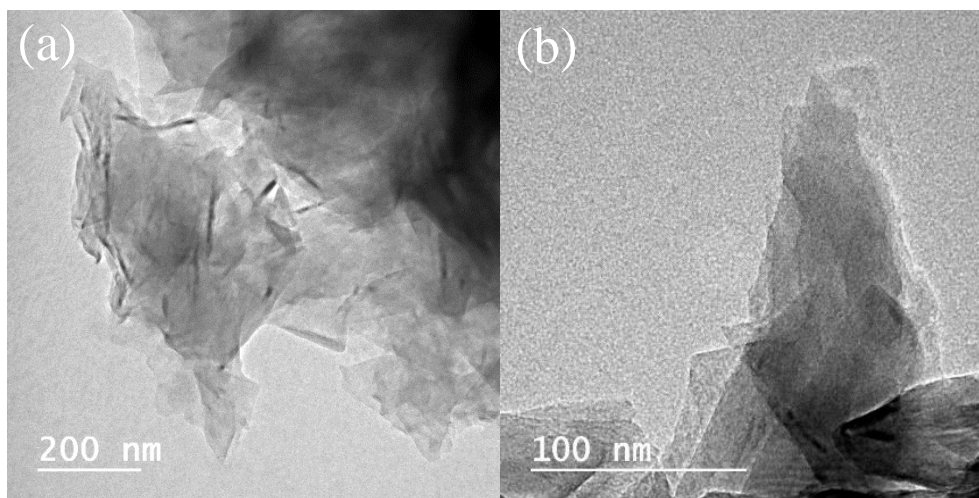
7

8
9

10   ***Figure 2****: TEM images of the dry employed nanopowders. (a) S-GnP nanopowder and (b) P-GnP*

11   *nanopowder.*

12

13   Previous works showed other structural information of these particles. Atomic force microscopy

14   analyses stated heights per graphene layer of 3 to 12 nm for S-GnP [50] and 2 to 18 nm for P-GnP

15   [51], so there are not significant differences in this dimension. Regarding chemical composition,

16   Energy-Dispersive X-ray Spectroscopy analyses showed the presence of carbon (C), oxygen (O) and

17   sulfur (S) for S-GnP [52] and carbon (C), oxygen (O) and potassium (K) for P-GnP [53].

18   As for the zeta potential characterization, it should be reminded that the higher are the

19   electrostatic repulsion forces among the nanoadditives, the higher the value of the zeta potential.

20   Usually, absolute zeta potential values over 30 mV are considered as a symptom of nanofluid stability

21   [46, 47, 54, 55], the higher the value, the greater the stability. (Table 1).

22

Z potential absolute value (mV)	Stability
0	No stability

15	Possible some stability but settling
30	Moderate stability
45	Good stability, possible settling
60	Very good stability, little settling likely

Table 1. *Relationships between zeta potential and stability [47].*

Figure 3 shows the results of the analysis of the zeta potential as a function of temperature for the 0.025 wt% samples, corresponding to the intermediate concentration among the three analysed. Error bars correspond to the standard deviation of the experimental data. As it can be observed, quasi-constant values were obtained for each nanofluid type, indicator of non-deterioration of samples at the studied temperatures. The mean values obtained were 43.8 and -53.3 mV for the P-GnP and S-GnP nanofluids, respectively. Both values are over the threshold of 30 mV of absolute value, synonym of moderate stability. Nevertheless, the value obtained for the S-GnP/water nanofluid is higher, even over 45 mV of absolute value (good stability, according with Table 1), indicating a potentially better behaviour than the P-GnP/water nanofluid.
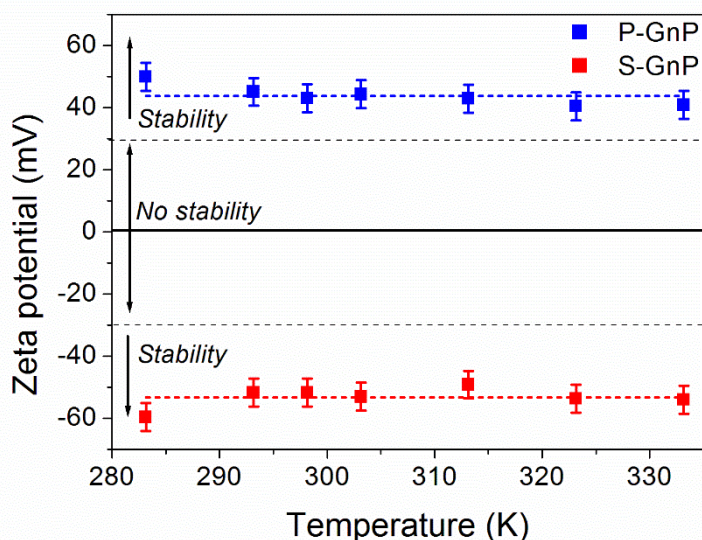

Figure 3: *Zeta potential dependence on temperature for the 0.025 wt% samples (red, S-GnP/water nanofluid; blue, P-GnP/water nanofluid).*

Figure 4 shows the size distribution by intensity for the 0.025 wt% S-GnP/water nanofluid and the 0.025 wt% P-GnP/water nanofluid just after preparation and one week after. It should be noted that dynamic light scattering measurements assume that nanoparticles are spherical while the

1   employed nanoadditives are nanoplatelets, so the reported size values should be considered as

2   "apparent" sizes. As it can be observed, in both cases the intensity peak is obtained for practically the

3   same apparent size for the samples measured just after preparation and the shaken samples 7 days

4   later. Nevertheless, the static samples 7 days after preparation showed intensity peaks at lower

5   apparent sizes, indication of the progressive sedimentation of larger nanoparticles. The decrease is

6   comparatively lower for the P-GnP nanofluid, in accordance with zeta potential results.

7
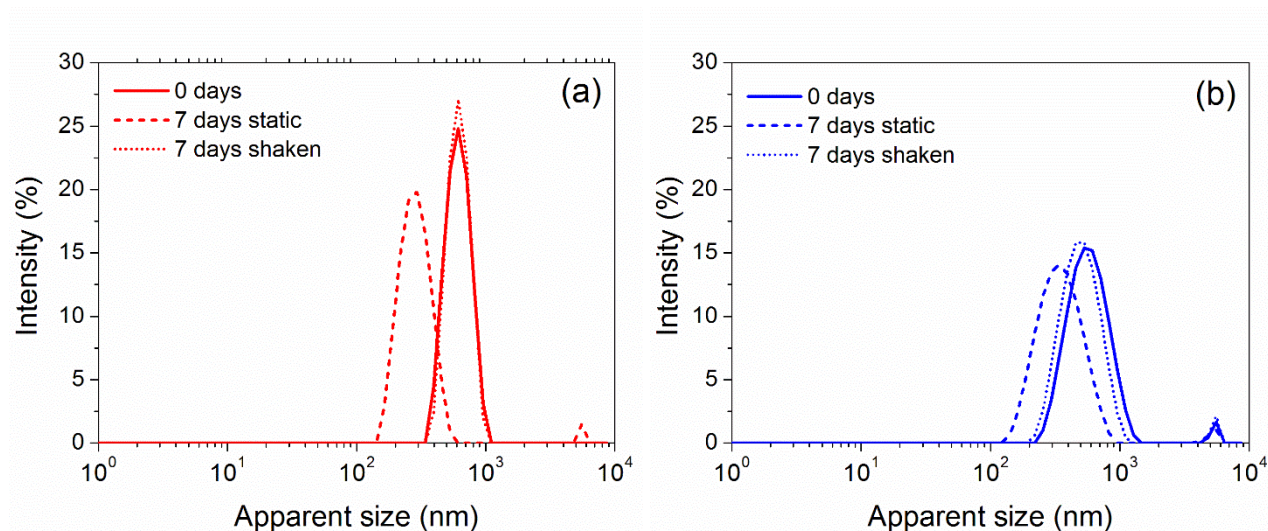
8

9   ***Figure 4****: Apparent size distribution for 0.025 wt% samples: (a) S-GnP/water nanofluid and (b) P-*

10   *GnP/water nanofluid.*

11

12   Figure 5 shows the Z-average size, i.e. the intensity-weighted mean size obtained from a

13   cumulants fit of the obtained autocorrelation function of intensity, as a function of the time after

14   preparation.

15   The evolution of the Z-average size shows again the quasi-constant value obtained for the shaken

16   samples, ~ 990 nm for S-GnP and ~ 540 nm for P-GnP. The static samples show again symptoms of

17   sedimentation with decreases up to ~ 360 nm for S-GnP and ~ 330 nm for P-GnP after seven days.

18   Furthermore, the lower decrease for the P-GnP nanofluid is evidenced and it should be noticed that

19   the value obtained for this sample 24 h after preparation is similar to the initial one.
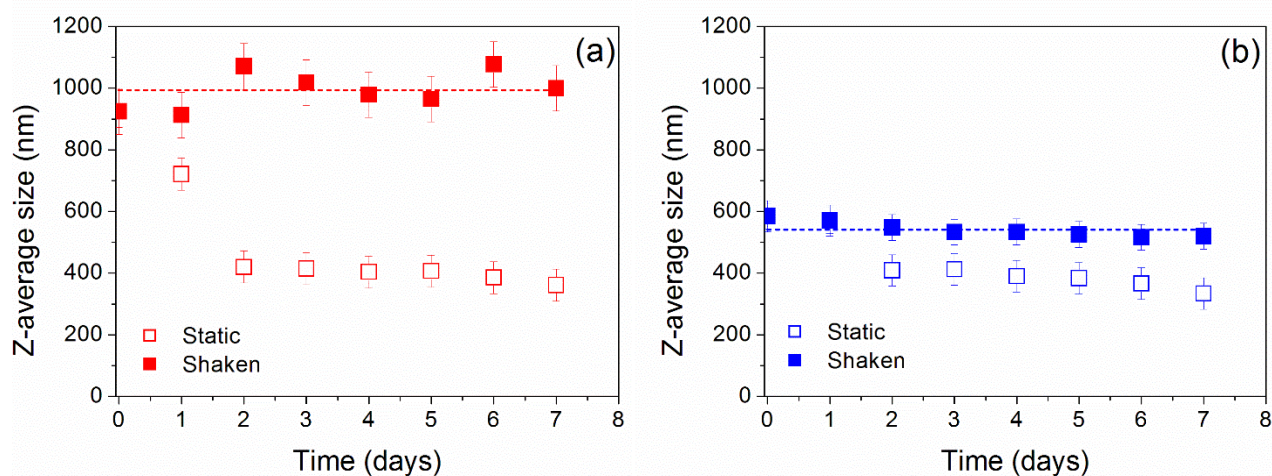
Figure 5: *Average Z-Size dependence on time after preparation for the 0.025 wt% samples. (a) S-GnP/water nanofluid and (b) P-GnP/water nanofluid.*

The complete stability analyses allow to conclude that moderately stable nanofluids were achieved with easily recoverable initial dispersion conditions. However, P-GnP/water nanofluids evidenced better long-term stability than S-GnP/water nanofluids.

3.2 Linear optical properties

Figures 6 and 7 show the experimental spectral extinction coefficient of P-GnP and S-GnP nanofluids, respectively. We can immediately observe that both nanoadditives show a higher extinction coefficient than water, especially in the UV, visible and near-infrared. Qualitatively speaking, both nanofluids show the typical UV plasmonic peak of the graphene-based nanostructures and an almost flat spectrum in the visible and near-infrared ranges [56]. The spectral features at around 1450 nm, 2000 nm and longer wavelengths are the water absorption bands; in particular the peak at around 2000 nm appears saturated, thus the height shown is not reliable. The enlargement of the 180-750 nm range in Fig. 6b allows to appreciate the spectrum of the sample at the lowest concentration. It is interesting to notice that P-GnPs extend their extinction tail in the whole investigated range, showing a well recognizable extinction coefficient increase even at the infrared local minima of water spectrum (around 1750 and 2250 nm). For the same values of nanopowder loading, the extinction coefficient is considerably higher in P-GnPs than in S-GnPs in the whole investigated wavelength range. Comparing both types of nanopowder, the shape of the UV plasmonic peak and of its tail appears different according to the different functionalization. Figure 8 shows the

10

1   nanopowder influence to the extinction coefficient of samples decoupled from that of the base fluid,

2   for the 0.025 wt% concentration. We can appreciate the higher and narrower plasmonic peak of P-

3   GnPs and their higher plateau value in the visible and infrared. In the region of sunlight spectrum,

4   which starts from 300 nm on, for the same concentration, P-GnPs show a nearly double extinction

5   coefficient than S-GnPs, resulting in a better solar absorber. However also S-GnPs can achieve a

6   comparable solar absorbance if a higher nanoparticle concentration will be taken into account.
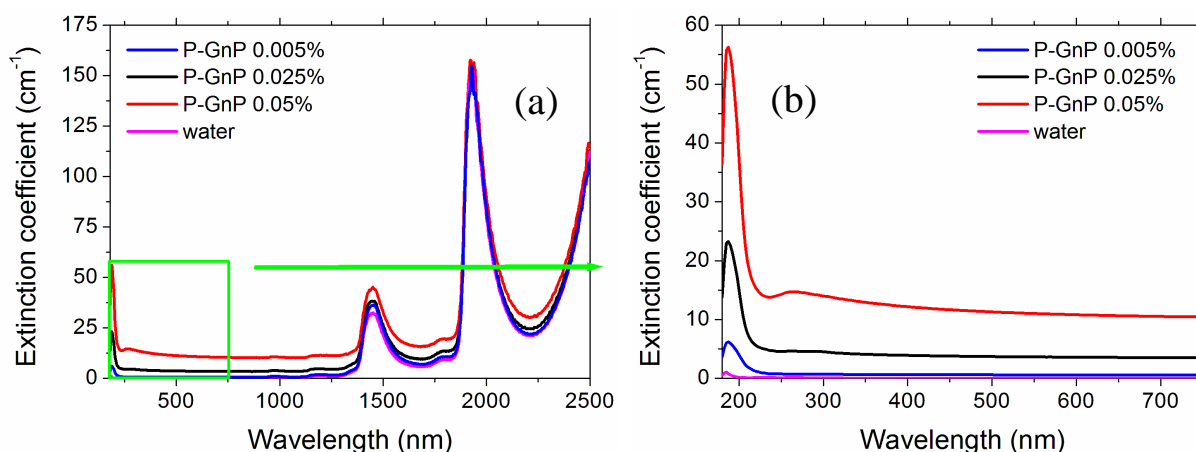
7
8
9   *Figure 6: Spectral extinction coefficient of P-GnP-based nanofluids with concentrations ranging*

10   *from 0.005 wt% to 0.05 wt%. The water extinction coefficient is also reported for reference.*
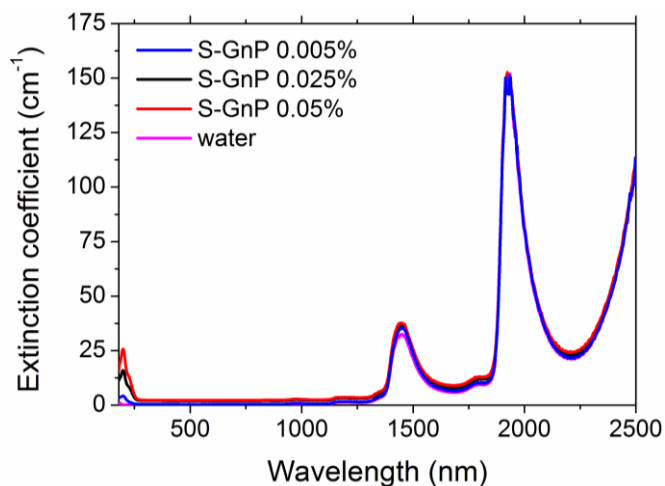
11
12   *Figure 7: Spectral extinction coefficients of S-GnP-based nanofluids at 0.025 wt% and 0.05 wt%*

13   *concentrations. The water extinction coefficient is also reported for reference.*
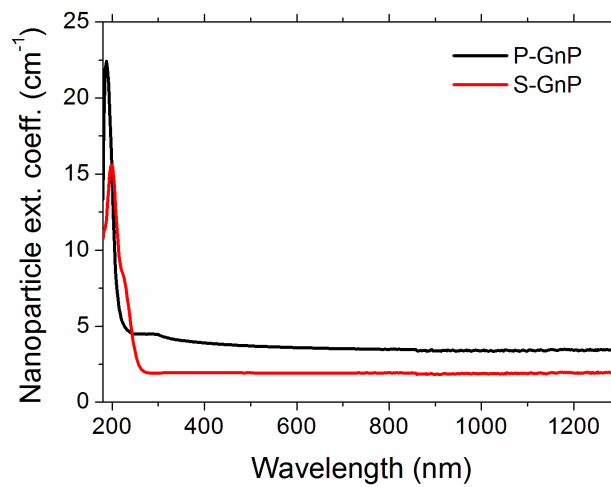
1
2   ***Figure 8****: Comparison of the nanoadditive contribution to the spectral extinction coefficients of*
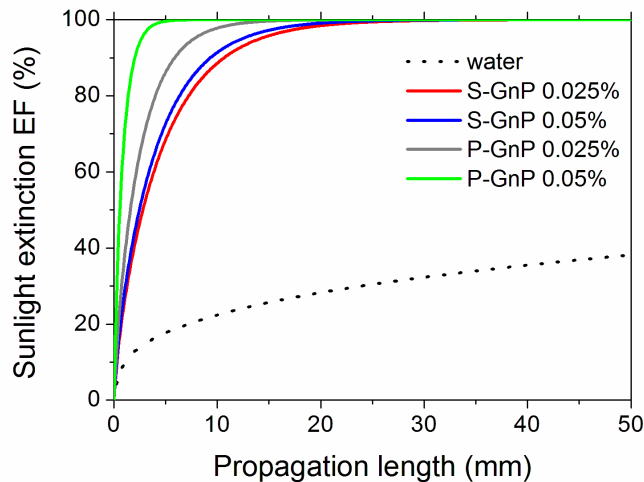3   *nanofluids.*

4

5   The evidenced spectral properties result extremely important to characterize the sunlight
6   extinction behavior of the nanofluids and their energy storage capability. The sunlight extinction
7   fraction, EF, of the incident sunlight I(λ) [57] which is extinct in the fluid after a propagation path of
8   length x is given by the expression [20, 25]:

9      $$EF(x) = 1 - \frac{\int_{\lambda_{min}}^{\lambda_{MAX}} I(\lambda) \cdot e^{-\mu(\lambda)x} d\lambda}{\int_{\lambda_{min}}^{\lambda_{MAX}} I(\lambda) d\lambda}$$ (1)

10   where $\mu(\lambda)$ is the spectral extinction coefficient and λ_{min} and λ_{MAX} are 300 and 2500 nm,
11   respectively.
12   Figure 9 compares the calculated EF fraction for the investigated nanofluids at the concentrations
13   of interest for solar absorber applications (0.025 wt% and 0.05 wt%) to that of the base fluid. We can
14   see how the addition of the different kinds of functionalized graphene nanoplatelets dramatically
15   modifies the interaction of the fluid with solar radiation, producing an almost complete sunlight
16   extinction after a path length, which, depending on the nanoadditive type and concentration, ranges
17   from 5 to 30 mm. This modification indicates that the light extinction after a path as long as 50 mm
18   in the nanofluids is about 250% higher than that of pure water. As expected from the small differences
19   in the extinction spectra, doubling the concentration in S-GnPs decreased the length for 99% sunlight
20   extinction only by about 3 mm (from 22 to 19 mm), while the concentration doubling in P-GnPs more
21   heavily affected the extinction length (99% extinction length shortened from about 12 to 4 mm), in

1   agreement with the largest differences in the spectral extinction coefficient shown by these

2   nanoadditives (Figure 6).

3

4   ***Figure 9****: Calculated sunlight extinction as a function of the propagation length within the*
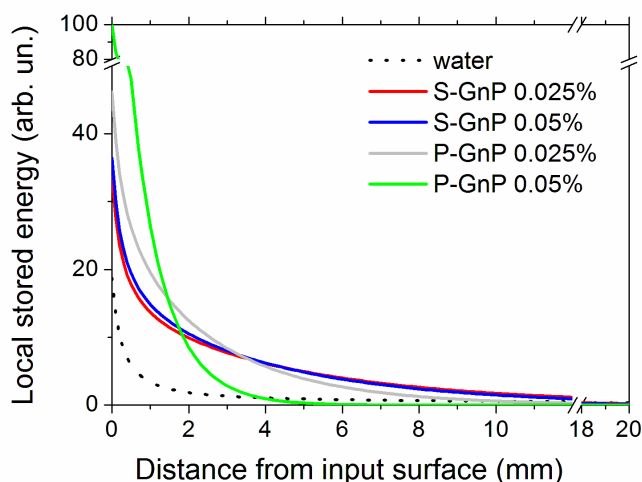
5   *nanofluids.*

6   It has to be considered that the type and concentration of nanoadditives also affect the spatial

7   distribution S(x) of the stored energy inside the nanofluid volume. This distribution, for a cold fluid

8   in absence of convective mixing is given by the expression:

9

10
$$S(x) = \frac{\int_{\lambda_{min}}^{\lambda_{MAX}} I(\lambda) \cdot \mu(\lambda) \cdot e^{-\mu(\lambda)x} d\lambda}{\int_{\lambda_{min}}^{\lambda_{MAX}} I(\lambda) d\lambda} \tag{2}$$

11

12   Plots of the calculated stored power distributions along the light propagation direction are reported

13   in Figure 10. Distributions refer to a single-sided irradiated nanofluid as in the case of a generic radial

14   direction in transverse section of the absorber tube in a sunlight parabolic-linear collector, or in the

15   case of the thickness direction in a flat-plate collector. The curves in Fig. 10 have been respectively

16   normalized referring to the highest value of the distribution for the 0.05 wt% P-GnP sample, thus they

17   have the meaning of relative values. As we can see (Fig. 10), the higher are extinction coefficients,

18   the more localized is sunlight extinction in the first layers of fluid. For the highest concentration P-

19   GnP sample, the energy is stored in a very small depth near the surface and inner layers are not

20   directly heated by the light at all, resulting in a strong distribution gradient. As the nanoadditive

21   concentration decreases, the stored energy distribution penetrates more deeply in the sample,

13

1   producing, after the first steep gradient, a uniform profile in the inner layers. For S-GnPs samples,

2   sunlight penetrates even more deeply in the volume, and further internal layers can be heated. As

3   apparent from Fig. 10, the energy distribution for pure water is lower than those of all nanofluid

4   samples, even for the less-concentrated S-GnPs nanofluid. As a final comment of this section, it is

5   important to notice that both the sunlight extinction and the stored energy distribution can be tailored

6   and adapted to the system geometry by tuning the extinction coefficient. That is possible adjusting

7   the concentration and/or the type of nanoparticles. In fact, the literature reports, for solar collectors

8   allowed to operate under optimal conditions both as for the nanofluid and the system architecture

9   design, efficiency increases from 5 to 10% with respect to surface solar absorbers [58-60].

10
11   ***Figure 10****: Stored energy distribution in the nanofluids as a function of the distance from the*

12   *sunlight input surface.*

13

14   **3.3 Nonlinear optical properties**

15

16   Due to the high extinction coefficient of the samples with 0.05 wt% nanoadditive concentration,

17   preventing any transmitted signal to be recorded at the output after the 10-mm length cell, high

18   intensity experiments were carried out on the lower 0.005 wt% and 0.025 wt% concentrations.

19   Figures 11 and 12 show the wavelength-dependent output energy measurements for the two

20   investigated concentrations for both nanofluid types. All samples show a marked nonlinear behaviour.

21   At 355 and 532 nm, the samples with the lowest concentration show a classical optical limiting

22   behaviour characterized by no sign inversion in the concavity of the curve deviating from linearity

1 and by an asymptotic-like trend, which is more recognizable, within the investigated energy range, in

2 P-GnP-based suspensions. At 1064 nm, where the laser is able to supply the highest energy, the larger

3 energy range experimentally accessible reveals a concavity change which, in carbon-nanohorn based

4 suspensions, was explained in terms of laser-induced sample damage [61]. In all cases, the P-GnP

5 samples show both the lowest starting linear transmittance and the most pronounced nonlinearity.

6   The higher 0.025 wt% concentration shows, for both samples and at all wavelengths, a more

7 complex nonlinear behaviour, with a non-monotonic trend as a function of the input energy,

8 characterized by a decrease after a local maximum, and, for the sample S-GnPs at 1064 nm, even by

9 a further increase for input energy higher than 10 mJ. Moreover, the two samples show very large

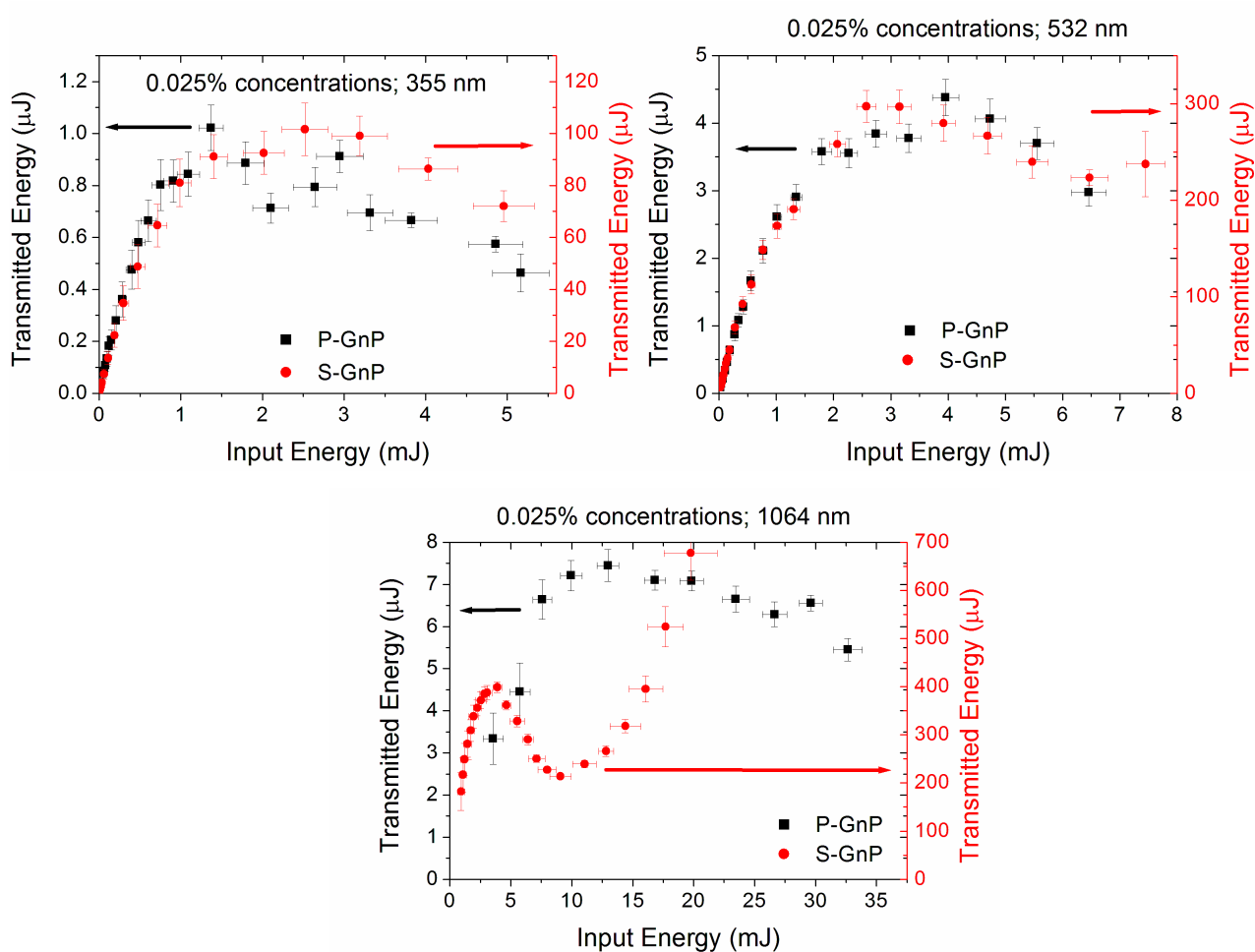10 difference in transmitted energy, so that two different ordinate axes are used.
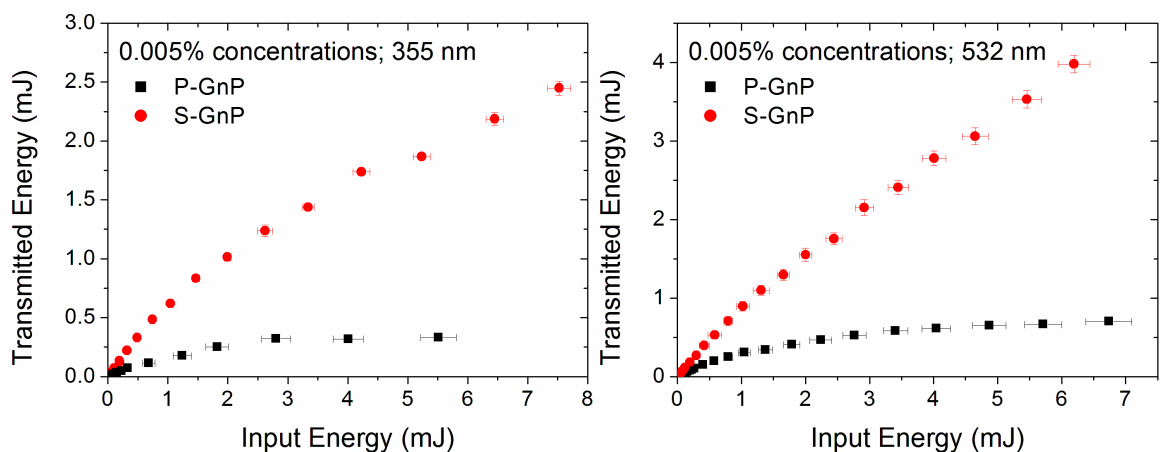
11
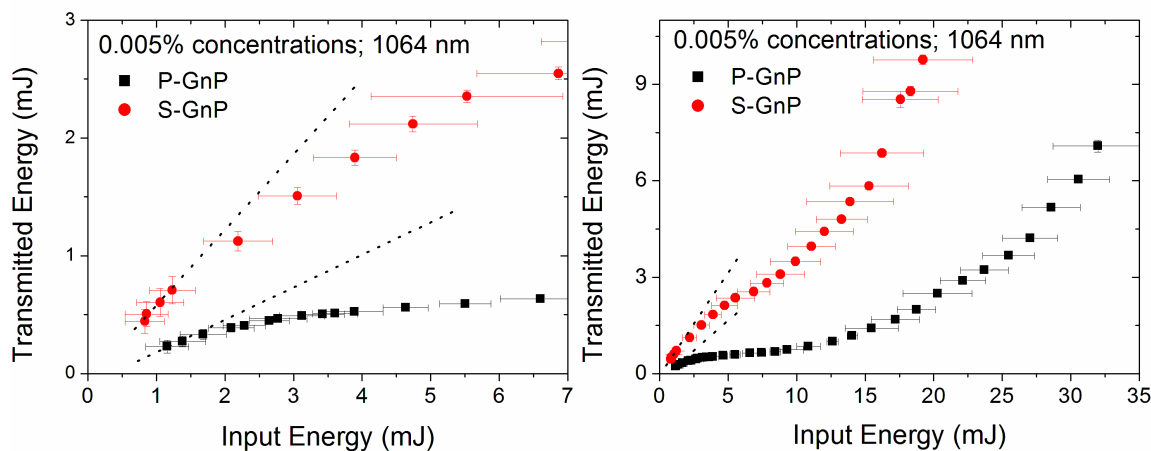
12
13

1   ***Figure 11.*** *Transmitted energy as a function of the incident energy under different wavelengths and*

2   *for the 0.005 wt% nanoadditive concentrations. The lower plots are both referred to the 1064 nm*

3   *wavelength (the dotted lines are a visual reference of the linear regime).*

4

5

6

7

8

9
10

11   ***Figure 12.*** *Transmitted energy as a function of the incident energy under different wavelengths and*

12   *for the 0.025 wt% nanoadditive concentrations.*

13

14   Figure 13 compares, for fixed nanoparticle type and concentration, the effect of changing the

15   laser wavelength. At all wavelengths and concentrations, the energy transmitted by P-GnP samples

16   is considerably lower than that of the corresponding S-GnP sample, in agreement with the lower

1   linear extinction coefficient, and, as noticed above, the nonlinearity is more pronounced. For fixed

2   nanoadditive type, the wavelength-dependent nonlinear behavior changes with the concentration. In

3   fact, even if the minimum transmittance is always obtained at 355 nm, the relative hierarchy of green

4   and infrared wavelength changes with the concentration. This seems to suggest different nonlinear

5   mechanisms acting at the lowest and highest concentration, at least for 532 nm and 1064 nm

6   wavelength. Moreover, for fixed sample and concentration, it is interesting to notice that the minimum

7   detectable output power is higher at 1064 nm than at 532 nm, despite that the linear extinction

8   coefficient at these wavelengths shows similar values, again suggesting a stronger nonlinearity, or, at

9   least, a lower nonlinearity energy threshold at 1064 nm.
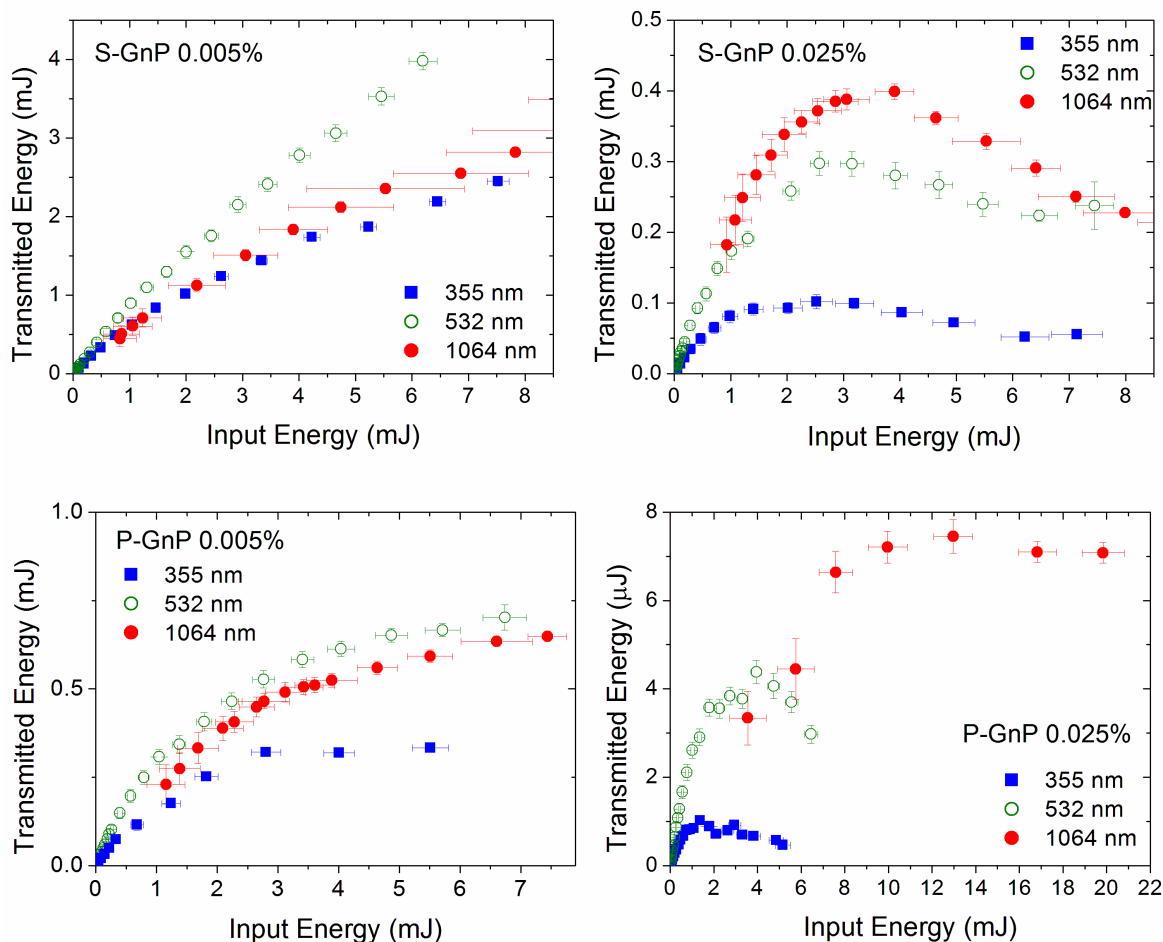
10

11
12

13   ***Figure 13.*** *Transmitted energy as a function of the incident energy for fixed nanoadditive type*

14   *and concentration.*

15

1 The phenomenon of optical limiting in colloids can be explained by two mechanisms: nonlinear

2 absorption or nonlinear scattering [62], depending on the nature of nanoparticles and on the properties

3 of the suspending fluids [63]. The effect actually occurring can be identified applying semi-empirical

4 models. Nonlinear absorption can be due to different effects like reverse saturable absorption, two-

5 photon absorption etc [63]. It can modeled introducing a nonlinear term in the Lambert-Beer law

6 [64]:

7 $$\frac{dF(z)}{dz} = -\mu F - \frac{\mu \sigma_1}{2\hbar\omega} F^2 \qquad (3)$$

8 where F(z) is the energy fluence at the z position in the sample, μ is the linear extinction coefficient,

9 σ_1 is the Excited State Absorption (ESA) cross section. If we solve this equation following the method

10 described in [65, 66], we can link the output energy from the nanofluid, E_{out}, to incident energy E_{in},

11 obtaining the following relationship:

12 $$E_{out} = \frac{T_s^2 e^{-\mu L} E_{in}}{1 + 0.1\, E_{in}/E_t} \qquad (4)$$

13

14 Where T_s^2 is a coefficient describing the reflection losses on the walls of the cuvette and L is the

15 thickness of the sample. The term $e^{-\mu L}$ describes the linear extinction, and E_t is the threshold energy

16 defined as the energy where the transmittance decreases to the 90% of its original value [64]. This

17 model will be identified as LB in the following.

18

19 On the other hand, a model where optical limiting is only due to nonlinear refraction has been

20 developed in [67]. In the cited reference, nonlinear properties are ascribed to nonlinear scattering

21 between laser photons and vapor bubbles yielded by the vaporization of the base fluid surrounding

22 the nanoparticle and/or by ionization and vaporization of the nanoparticles:

23 $$E_{out} = T_s^2 E_t\, e^{-\mu L} \left(1 + \frac{\mu^e}{\mu} \left(\frac{E_{in}}{E_t} - 1 \right) \right)^{\frac{\mu}{\mu^e}} \qquad (5)$$

24 where μ^e is the nonlinear extinction coefficient and E_t is the energy threshold for bubble formation,

25 both obtained from a fitting procedure of experimental data. This model is labelled as MMJ in the

26 following.

27

1 A series of numerical tests were carried out to verify whether theoretical models are compatible with

2 our experimental data, and, in the positive case, to estimate the values of the model parameters. The

3 procedure consisted in a standard least-squares approach, where the objective function is the sum S

4 of the squared differences between the observed E_{out} values and the corresponding computed values

5 for each E_{in}, as described in Ref. [61].

6   None of the considered models can reproduce non-monotonic nonlinear trends, which require

7 thus further investigation. The cases when the fitting was successful are shown in Figure 14. We can

8 see that, except the case 0.005 wt% S-GnP and 532 nm, the only acceptable model is the nonlinear

9 Lambert-Beer (Eq. 4). Table 2 lists the obtained energy threshold values. If we compare the values

10 obtained from the nonlinear Lambert-Beer model, we can see that the threshold increases with the

11 wavelength and that it is always lower in P-GnPs than in S-GnPs samples. In the only case when

12 fitting by the MMJ model was acceptable, we can see that the MMJ threshold value is one order of

13 magnitude lower than the Lambert-Beer one. This result is not surprising, because the two models

14 account for different physical phenomena (nonlinear absorption and nonlinear refraction).
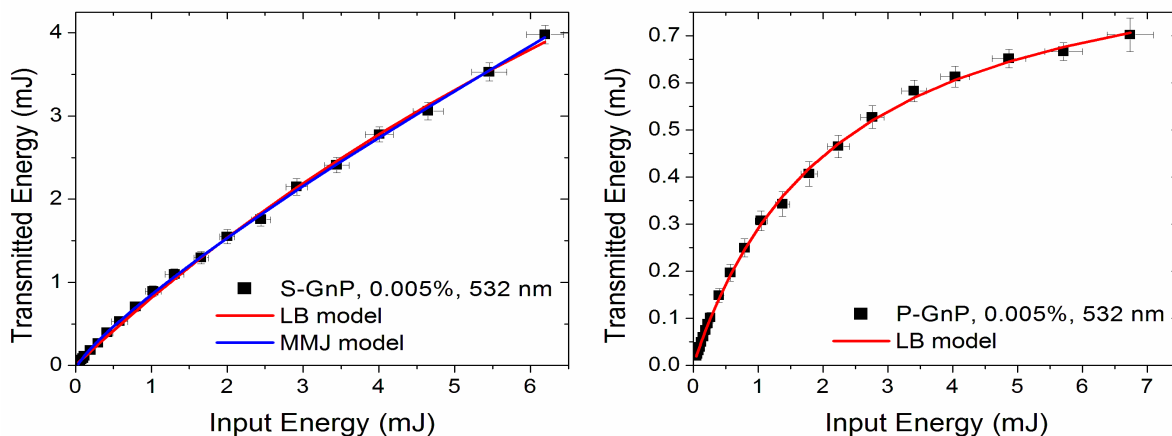
15
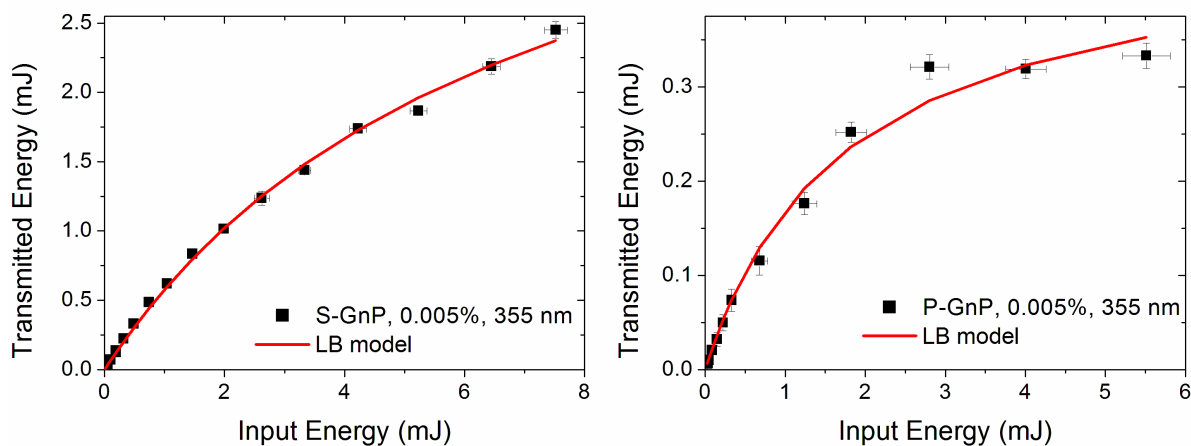
16
17

Figure 14. *Fitting of experimental data with Eqs. 4 and 5.*

Sample, concentration	Wavelength (nm)	Energy threshold (mJ), model
0.005 wt%, P-GnPs	355	0.18 ± 0.02, LB
	532	0.22 ± 0.02, LB
0.005 wt%, S-GnPs	355	0.70 ± 0.08, LB
	532	1.7 ± 0.5, LB 0.17 ± 0.02, MMJ

Table 2. *Energy threshold values obtained from the semi-empirical model fitting.*

4. Conclusions

Two different nanosuspensions of polycarboxylate chemically modified graphene nanoplatelets (P-GnP) and Sulfonic acid-functionalized graphene nanoplatelets (S-GnP) dispersed in water were tested, at three different concentrations (0.005 wt%, 0.025%wt and 0.05 wt%). Dispersions, and especially P-GnP, showed a satisfying long-term stability. Spectrophotometric measurements allowed to obtain the spectral extinction coefficients and to evaluate the potential for direct solar absorber applications. For both colloid types, the sunlight radiation is nearly completely extinguished in 5-20 mm path length, with the differences among the samples connected to the concentration and to the different functionalization of nanoadditives. The nonlinear optical measurements, carried out on 0.005 wt% and 0.025% wt concentrations, evidenced a non-linear behaviour for both nanoadditive types, both concentrations, and at all the three test wavelengths (ultra-violet, visible, and near-infrared), demonstrating appealing broadband characteristics. Fitting of nonlinear data with semi-

empirical models showed thresholds between 0.18 and 1.7 mJ, and the prevalence of nonlinear absorption effects for the lowest concentrations. More marked and non-monotonic nonlinear behaviours were obtained at the highest concentrations, seeming to suggest the occurrence of concurrent nonlinear mechanisms, likely involving the production of bubbles. The energy densities reached in the experiments are compatible with solar concentration systems [68], thus opening interesting perspectives for the further application of these nanofluids in solar vapor generation and solar desalination [69].

Acknowledgments

References

[1] X. Huang, K. J. Prashant, I. H. El-Sayed, and M. A. El-Sayed, "Gold nanoparticles: interesting optical properties and recent applications in cancer diagnostics and therapy." Nanomedicine 2(5), 681 (2007).

[2] I. Sharifi, H. Shokrollahi, and S. Amiri, "Ferrite-based magnetic nanofluids used in hyperthermia applications." Journal of Magnetism and Magnetic Materials 324(6), 903 (2012).

[3] R. Taylor, S. Coulombe, T. Otanicar, P. Phelan, A. Gunawan, W. Lv, G. Rosengarten, R. Prasher, and H. Tyagi, "Small particles, big impacts: a review of the diverse applications of nanofluids." Journal of Applied Physics 113, 011301 (2013).

[4] P. D. Howes, R. Chandrawati, and M. M. Stevens, "Colloidal nanoparticles as advanced biological sensors." Science 346(6205), 1247390 (2014).

[5] X. Fan, and I. M. White, "Optofluidic microsystems for chemical and biological analysis." Nature Photonics 5(10), 591 (2011).

[6] L. Wang, W. Ma, L. Xu, W. Chen, Y. Zhu, C. Xu, and N. A. Kotov, "Nanoparticle-based environmental sensors." Materials Science and Engineering: R: Reports 70(3-6), 265 (2010).

[7] V. Mahendran, and J. Philip, "An optical technique for fast and ultrasensitive detection of ammonia using magnetic nanofluids." Applied Physics Letters 102(6), 063107 (2013).

[8] R. A. Taylor, T. P. Otanicar, Y. Herukerrupu, F. Bremond, G. Rosengarten, E. R. Hawkes, X. Jiang, and S. Coulombe, "Feasibility of nanofluid-based optical filters." Applied Optics 52(7), 1413 (2013).

[9] O. Ilic, I. Kaminer, Y. Lahini, H. Buljan, and M. Soljacic, "Exploiting optical asymmetry for controlled guiding of particles with light." ACS Photonics 3(2), 197 (2016).

[10] J. Li, J. Liu, X. Tian, and Z.-Y. Li, "Plasmonic Particles with Unique Optical Interaction and Mechanical Motion Properties." Particle & Particle Systems Characterization 34(8), 1600380 (2017).

[11] Khanafer, K., & Vafai, K., "A review on the applications of nanofluids in solar energy field". Renewable Energy, 123, 398-406 (2018).

[12] Bellos, E., Tzivanidis, C., Antonopoulos, K. A., & Gkinis, G., "Thermal enhancement of solar parabolic trough collectors by using nanofluids and converging-diverging absorber tube". Renewable Energy, 94, 213-222 (2016).

[13] T.P. Otanicar, P.E. Phelan, R.S. Prasher, G. Rosengarten, and R.A. Taylor, "Nanofluid-based direct absorption solar collector," Journal Renewable Sustainable Energy 2, 033102 (2010).

[14] R.A. Taylor, P.E. Phelan, T.P. Otanicar, R. Adrian, and R. Prasher, "Nanofluid optical property characterization: towards efficient direct absorption solar collectors," Nanoscale Research Letters 6, 225 (2011).

[15] Gorji, T. B., & Ranjbar, A. A., "Thermal and exergy optimization of a nanofluid-based direct absorption solar collector". Renewable Energy, 106, 274-287 (2017).

[16] Sharaf, O. Z., Al-Khateeb, A. N., Kyritsis, D. C., Abu-Nada, E., "Energy and exergy analysis and optimization of low-flux direct absorption solar collectors (DASCs): Balancing power-and temperature-gain". Renewable Energy, 133, 861-872 (2019).

[17] J.E. Minardi, H.N. Chuang, "Performance of a black liquid flat-plate solar collector", Solar Energy, 17, 179-183 (1975)

[18] U. Srivastva, R.K. Malhotra, S.C. Kaushik, "Recent developments in Heat Transfer Fluids used for solar thermal energy applications", J Fundam Renewable Energy Appl, 5, 189 (2015)

[19] Burke, A. R., D. E. Etter, C. R. Hudgens, C. J. Wiedenheft, and L. J. Wittenberg. "Thermal and photochemical studies of solar energy absorbers dissolved in heat transfer fluids." Solar Energy Materials 6, 481-490 (1982).

[20] E. Sani, L. Mercatelli, S. Barison, C. Pagura, F. Agresti, L. Colla, and P. Sansoni, "Potential of carbon nanohorn-based suspensions for solar thermal collectors," Solar Energy Materials and Solar Cells 95 2994 (2011).

[21] Z. Luo, C. Wang, W. Wei, G. Xiao, and M. Ni, "Performance improvement of a nanofluid solar collector based on direct absorption collection (DAC) concepts," International Jounal Heat and Mass Transfer 75, 262 (2014).

[22] M. Karami, M.A. Bahabadi, S. Delfani, and A. Ghozatloo, "A new application of carbon nanotubes nanofluid as working fluid of low-temperature direct absorption solar collector," Solar Energy Materials and Solar Cells 121, 114 (2014).

[23] S. Delfani, M. Karami, and M. Akhavan-Behabadi, "Performance characteristics of a residential-type direct absorption solar collector using MWCNT nanofluid," Renewable Energy 87, 754 (2016).

[24] T.B. Gorji, A. Ranjbar, and S. Mirzababaei, "Optical properties of carboxyl functionalized carbon nanotube aqueous nanofluids as direct solar thermal energy absorbers," Solar Energy 119, 332 (2015).

[25] E. Sani, S. Barison, C. Pagura, L. Mercatelli, P. Sansoni, D. Fontani, D. Jafrancesco, and F. Francini, "Carbon nanohorns-based nanofluids as direct sunlight absorbers," Optics Express 18, 5179 (2010).

[26] A. Moradi, E. Sani, M. Simonetti, F. Francini, E. Chiavazzo, and P. Asinari, "Carbon-nanohorn based nanofluids for a direct absorption solar collector for civil application," Journal of Nanoscience and Nanotechnology, 15, 3488 (2015).

[27] L. Mercatelli, E. Sani, A. Giannini, P. Di Ninni, F. Martelli, and G. Zaccanti, "Carbon nanohorn-based nanofluids: characterization of the spectral scattering albedo," Nanoscale Research Letters 7, 96 (2012).

[28] A.K. Geim and K.S. Novoselov, "The rise of graphene," Nature Materials 6, 183 (2007).

[29] Liu, J., Wang, F., Zhang, L., Fang, X., & Zhang, Z.,Thermodynamic properties and thermal stability of ionic liquid-based nanofluids containing graphene as advanced heat transfer fluids for medium-to-high-temperature applications. Renewable Energy, 63, 519-523 (2014).

[30] Y. Si and E. T. Samulski, "Synthesis of Water Soluble Graphene," Nano Letters 8, 1679 (2008).

[31] S. Park, J. An, R. D. Piner, I. Jung, D. Yang, A. Velamakanni, S. T. Nguyen, and R. S. Ruoff, "Aqueous Suspension and Characterization of Chemically Modified Graphene Sheets," Chemistry of Materials 20, 6592 (2008).

[32] M.A. Shannon, P.W. Bohn, M. Elimelech, J. G. Georgiadis, B.J. Mariñas, and A. M. Mayes, "Science and technology for water purification in the coming decades," Nature 452, 301 (2008).

[33] Ravaghi-Ardebili, Z., Manenti, F., Corbetta, M., Pirola, C., & Ranzi, E., "Biomass gasification using low-temperature solar-driven steam supply". Renewable energy, 74, 671-680 (2015).

[34] G.N. Tiwari, H.N. Singh, and R. Tripathi, "Present status of solar distillation," Solar Energy 75, 367 (2003).

[35] M. Elimelech and W.A. Phillip, "The future of seawater desalination: energy, technology, and the environment," Science 333, 712 (2011).

[36] C.Li, Y. Goswami, and E. Stefanakos, "Solar assisted sea water desalination: A review," Renewable and Sustainable Energy Reviews 19, 136 (2013).

[37] E. Zarza, M.E. Rojas, L. Gonzalez, J.M. Caballero, and F. Rueda, "INDITEP: The first pre-commercial DSG solar power plant," Solar Energy 80, 1270 (2006).

[38] H. Nezammahalleh, F. Farhadi, and M. Tanhaemami, "Conceptual design and techno-economic assessment of integrated solar combined cycle system with DSG technology,". Solar Energy 84, 1696 (2010).

[39] A.S. Gudekar, A.S. Jadhav, S.V. Panse, J.B. Joshi, and A.B. Pandit, "Cost effective design of compound parabolic collector for steam generation," Solar Energy 90, 43 (2013).

[40] O. Neumann, A.S. Urban, J. Day, S. Lal, P. Nordlander, and N.J. Halas, "Solar vapor generation enabled by nanoparticles," ACS Nano 7, 42 (2012).

[41] H. Jin, G. Lin, L. Bai, A. Zeiny, and D. Wen, "Steam generation in a nanoparticle-based solar receiver," Nano Energy 28, 397 (2016).

[42] O. Neumann, C. Feronti, A.D. Neumann, A. Dong, K. Schell, B. Lu, E. Kim, M. Quinn, S. Thompson, N. Grady, and P. Nordlander, "Compact solar autoclave based on steam generation using broadband light-harvesting nanoparticles", Proceedings of the National Academy of Sciences, 110, 11677 (2013).

[43] S. Ishii, R.P. Sugavaneshwar, K. Chen, T.D Dao, and T. Nagao, "Solar water heating and vaporization with silicon nanoparticles at Mie resonances," Optical Materials Express 6, 640 (2016).

[44] G. Ni, N. Miljkovic, H. Ghasemi, X. Huang, S.V. Boriskina, C.T. Lin, J. Wang, Y. Xu, M.M. Rahman, T. Zhang, and G. Chen, "Volumetric solar heating of nanofluids for direct vapor generation," Nano Energy 17, 290 (2015).

[45] X. Wang, G. Ou, N. Wang, and H. Wu, "Graphene-based recyclable photo-absorbers for high-efficiency seawater desalination," ACS Applied Materials & Interfaces 8, 9194 (2016).

[46] Babita, S. K. Sharma and S.M. Gupta, "Preparation and evaluation of stable nanofluids for heat transfer application: a review," Experimental Thermal and Fluid Science 79, 202 (2016).

[47] A. Ghadimi, R. Saidur, and H. Metselaar, "A review of nanofluid stability properties and characterization in stationary conditions," International Journal of Heat and Mass Transfer 54, 4051 (2011).

[48] E. Sani and A. Dell'Oro, "Optical constants of ethylene glycol over an extremely wide spectral range," Optical Materials 37, 36 (2014).

[49] E. Sani and A. Dell'Oro, "Spectral optical constants of ethanol and isopropanol from ultraviolet to far infrared," Optical Materials 60, 137 (2016).

[50] J. P. Vallejo, S. Gómez-Barreiro, D. Cabaleiro, C. Gracia-Fernández, J. Fernández-Seara, and L. Lugo, "Flow behaviour of suspensions of functionalized graphene nanoplatelets in propylene glycol–water mixtures", International Communications in Heat and Mass Transfer 91, 150 (2018).

[51] J. P. Vallejo, G. Żyła, J. Fernández-Seara, and L. Lugo, "Rheological behaviour of functionalized graphene nanoplatelet nanofluids based on water and propylene glycol: water mixtures," International Communications in Heat and Mass Transfer 99, 43 (2018).

[52] R. Agromayor, D. Cabaleiro, A. A. Pardinas, J. P. Vallejo, J. Fernandez-Seara, and L. Lugo, "Heat transfer performance of functionalized graphene nanoplatelet aqueous nanofluids," Materials 9, 455 (2016).

[53] J. P. Vallejo, E. Álvarez-Regueiro, D. Cabaleiro, J. Fernández-Seara, J. Fernández, and L. Lugo, "Functionalized graphene nanoplatelet nanofluids based on a commercial industrial antifreeze for the thermal performance enhancement of wind turbines", Applied Thermal Engineering, submitted (2019)

[54] J.H. Lee, K.S. Hwang, S.P. Jang, B.H. Lee, J.H. Kim, S.U.S. Choi, C.J. Choi, "Effective viscosities and thermal conductivities of aqueous nanofluids containing low volume concentrations of Al2O3 nanoparticles", Int. J. Heat Mass Transfer 51, 2651–2656 (2008).

[55] L. Vandsburger, "Synthesis and Covalent Surface Modification of Carbon Nanotubes for Preparation of Stabilized Nanofluid Suspensions", M.Eng., McGill University (Canada), Canada, 2009.

[56] E. Sani, J. P. Vallejo, D. Cabaleiro, and L. Lugo, "Functionalized graphene nanoplatelet-nanofluids for solar thermal collectors," Solar Energy Materials and Solar Cells 185, 205 (2018).

[57] Standard Tables for Reference Solar Spectral Irradiances: Direct Normal and Hemispherical on 37° Tilted Surface, Active Standard ASTM G173. ASTM G173 - 03 (2012).

[58] Taylor, R.A., Phelan, P.E., Otanicar, T.P., Walker, C.A., Nguyen, M., Trimble, S. and Prasher, R. "Applicability of nanofluids in high flux solar collectors". Journal of Renewable Sustainable Energy, 3, 023104-1/15 (2011).

[59] Tyagi, H., Phelan, P., & Prasher, R. "Predicted efficiency of a low-temperature nanofluid-based direct absorption solar collector". Journal of Solar Energy Engineering, 131, 041004 (2009).

[60] Dugaria, S., Bortolato, M., & Del Col, D. (2018). Modelling of a direct absorption solar receiver using carbon based nanofluids under concentrated solar radiation. Renewable Energy, 128, 495-508.

[61] E. Sani, N. Papi, L. Mercatelli, S. Barison, F. Agresti, S. Rossi, and A. Dell'Oro, "Optical limiting study of carbon nanohorn-based aqueous nanofluids," submitted (2019)

[62] D.J. Hagam, T. Xia, A.A Said, and E.W Van Stryland, "Tandem Limiter Optimization," In Nonlinear Optical Materials for Switching and Limiting, vol. 2229, 179. International Society for Optics and Photonics, 1994.

[63] L.W. Tutt and A. Kost, "Optical limiting performance of C60 and C70 solutions," Nature 356 225 (1992).

[64] D. Vincent and J. Cruickshank, "Optical limiting with C60 and other fullerenes," Applied Optics 36, 7794 (1997).

[65] T. Pritchett, "Models for Saturable and Reverse Saturable Absorption in Materials for Optical Limiting," No. ARL-TR-2567, Army Research Laboratory (2002).

[66] D. Vincent, "Optical limiting threshold in carbon suspension and reverse saturable absorber materials," Applied Optics 40, 6646 (2001).

[67] K. J. McEwan, P.K. Milsom, and D.B James, "Nonlinear optical effects in carbon suspensions," In Nonlinear Optical Liquids for Power Limiting and Imaging, vol. 3472, 42. International Society for Optics and Photonics, 1998.

[68] S. A. Kalogirou, "Solar thermal collectors and applications," Progress in Energy and Combustion Science 30, 231 (2004).

[69] Zeiny, A., Jin, H., Lin, G., Song, P. and Wen, D., "Solar evaporation via nanofluids: A comparative study". Renewable Energy, 122 (2018) 443-454.